AIAA JOURNAL
Vol. 44, No. 7, July 2006

# Boundary-Layer Control with Atmospheric Plasma Discharges

Gabriel I. Font*
*U.S. Air Force Academy, Colorado 80840*

**Recent studies have investigated the use of plasma actuators for the active control of the boundary layer on turbine blades. Although the overall effects have been quantified through experiments, the exact nature of the plasma and its momentum-transfer mechanisms have not been well characterized. In this study, particle-in-cell and Monte Carlo methods are used to computationally explore the plasma discharge and its interaction with the flow. The plasma composition, its methods of momentum addition, and the physics of its generation are quantified. Comparisons with experiments are made in order to support the findings. Simulations indicate that the plasma is generated through an electron avalanche in a dielectric barrier discharge. The plasma is created as the electrons stream to the dielectric on the first half of the electrode bias cycle and stream back on the second half. Momentum is imparted to the flow on both half-cycles, but the ionization is not equal during both half-cycles. This results in the plasma actuator producing a net force in one direction.**

## I. Introduction

THE lift performance of an airfoil, as the angle of attack increases, is limited by the ability to maintain the boundary-layer attachment to the suction surface. When the chordwise pressure gradient becomes sufficiently large, the boundary layer loses its momentum and separates from the surface. Traditionally, vortex generators or pneumatic jets have been used to reenergize the boundary layer and promote attachment. A recently developed alternative utilizes a plasma to impart momentum to the boundary layer for the same result.[1–6] It has been successfully employed for boundary-layer separation control in airfoils and turbine blades.[2–5] It is called a plasma actuator and is effective in increasing lift and lowering drag.[4] The method consists of generating a plasma (ionized gas) in the boundary layer, which is in danger of separation. The ions and electrons accelerate in the electric field used to generate the plasma and then impart their momentum to the air molecules through collisions. The plasma, therefore, acts as a momentum source to the boundary layer allowing it to remain attached throughout a larger portion of the airfoil.

The plasma actuator consists of two long conducting (metal) strips placed parallel to each other (Fig. 1). The two strips act as electrodes and are arranged with a horizontal offset from each other. The lower electrode is covered with a dielectric, whereas the upper electrode is exposed to the flow. An alternating voltage is applied across the electrodes resulting in the generation of plasma in the vicinity of the electrodes. The voltage difference applied between the electrodes can vary from 1 kV to as high as 5 kV. The frequency of the driving voltage is typically from 1 to 10 kHz.

The creation of the plasma might be caused by one of two mechanisms. The first mechanism can be capacitive coupling,[7] where the electrons in the plasma gain energy by oscillating in the fluctuating electric fields in the sheaths. The sheaths can be thought of as electrical boundary layers that are created near surfaces as a result of the difference in the thermal velocities of the ions and the electrons. A capacitively coupled plasma is typically characterized by a spatially diffuse glow that persists uniformly in time over the multiple electrode bias cycles. This type of plasma is often used for materials processing at pressures of 1–10 torr (0.001–0.01 atm).

The second mechanism is an electron avalanche. In this mechanism, the electrons accelerate in an electric field and gain sufficient energy to cause ionization when they collide with the neutrals. The newly created electrons then accelerate in the field and cause further ionization. The result is a runaway cascade of ionization events. This type of plasma persists over a short time (nanoseconds) and is concentrated in a small space (fractions of millimeters). If this plasma is initiated with a broad electrode, millions of individual cascade events can combine to form what appears to be a uniform plasma. Experimental measurements taken with sufficient time resolution, however, will still reveal the individual electron avalanche events.[8–11] This type of plasma is typically used for materials processing at atmospheric pressures.[7]

Current measurements taken by Enloe et al.[6] (reproduced in Fig. 2) reveal individual current spikes at timescales that are more than 100 times faster than the electrode bias cycle. This is indicative of electron avalanches and not a capacitively coupled plasma, where the current measurements would follow the bias cycle. The plasma is also observed to extinguish (cease to exist) between each half of the bias cycle. This suggests that the plasma is regenerated by the electric field each time it changes direction. These two observations lead to the conclusion that the plasma actuator is working to generate plasma through electron avalanches. When the upper electrode is biased negatively, the electrons avalanche toward the buried electrode. Because the buried electrode is covered with a dielectric, the electrons are stopped from leaving and remain on the surface of the dielectric resulting in the extinguishing of the plasma. When the electric field reverses on the latter half of the bias cycle, the electrons are again accelerated (this time toward the exposed electrode) and regenerate the plasma through a second avalanche. This type of plasma discharge is commonly known as a dielectric barrier discharge.

## II. Computational Model

Simulation of the plasma was accomplished using a particle-in-cell direct-simulation Monte Carlo (PIC–DSMC) method. It has been exhaustively documented in the literature[12–17] and will be only briefly discussed here. In the PIC method, a single computational particle represents thousands or millions of charged particles of one species (ion or electron). The particle motion is updated in time as influenced by the forces caused by the electric fields. The electric fields are calculated by differentiating the electric potential, which is computed by solving the Poisson's equation. The charge distribution for the solution of the Poisson's equation is determined from the particle positions. A plasma is characterized by following the behavior of thousands or millions of computational particles. At each time step, the force is calculated on each particle from the local electric fields. The velocities are then updated from the forces and

Presented as Paper 2004-3574 at the AIAA/ASME/SAE/ASEE 40th Joint Propulsion Conference, Fort Lauderdale, FL, 11–14 July 2004; received 1 July 2005; revision received 28 September 2005; accepted for publication 23 November 2005. 

*Professor, Department of Physics. Member AIAA.

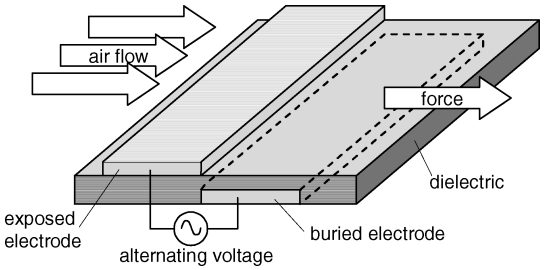


**Fig. 1 Plasma-actuator configuration.**

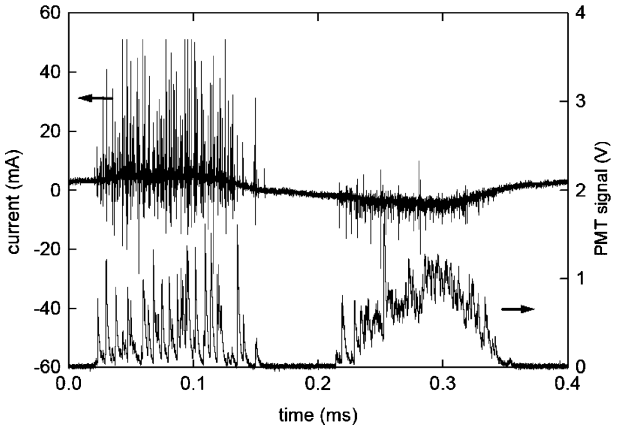


**Fig. 2 Current and light emission (PMT signal) from plasma-actuator discharge. Reproduced from Ref. 6.**

new particle positions are computed using a leap-frog method.[12] A new charge distribution is then determined from the updated particle positions, and the electric potential and resulting electric fields are computed from the new charge distribution. The method is repeated at each time step. In the present simulation, both ions and electrons are treated as computational particles.

The plasma actuator operates at atmospheric pressure. Because of the high air density, the collisions between the plasma particles and the neutral (air) molecules cannot be ignored. For this reason, a Monte Carlo[16,17] method was used to evaluate the collision events. A no-time-counter method[16] is utilized during each time step to determine which ions and electrons have collided with the air molecules. Any chemistry that can take place as a result of the collision is also evaluated. Any momentum transfer is recorded, and any chemical change caused by a collisional event is used to update the concentration of species in the cell. Because the electron avalanche takes place in tens of nanoseconds, the neutrals do not have sufficient time to move any significant distance. Therefore, the neutrals are treated as a background component of the simulation, and their motion is not modeled.

The simulation is conducted in pure nitrogen. The oxygen in the air is thought to significantly alter the discharge caused by the presence of negative ($O-$) ions. This leads to different ion recombination behavior, altered sheath structure, and perhaps, even different force production characteristics. In the interest of understanding the physics of the discharge, however, the simpler case of pure nitrogen is examined in the present study. The addition of oxygen and its associated chemistry will be made in future studies.

The chemical reactions allowed in the present study are shown in Table 1. They include electron momentum transfer, molecular ionization, excitation, and dissociation. It also includes nitrogen molecule momentum transfer and charge exchange. These last two reactions will be the primary mechanism for momentum transfer (force) to the neutrals. Electron momentum transfer is important in correctly calculating the energy of the electrons but does not significantly affect momentum transfer to the neutrals. No rate constants were used in calculating the reactions. Instead, the collision cross sections from Ref. 18 were used directly to determine the probability of any collision event taking place.

**Table 1 Chemical reactions in the simulation**

| Reaction | Description |
|---|---|
| $e + N_2 \rightarrow N_2 + e$ | Momentum transfer |
| $e + N_2 \rightarrow N_2^+ + 2e$ | Ionization |
| $e + N_2 \rightarrow N_2^* + e$ | Excitation |
| $e + N_2 \rightarrow 2N + e$ | Dissociation |
| $N_2^+ + N_2 \rightarrow N_2^+ + N_2$ | Momentum transfer |
| $N_2^+ + N_2 \rightarrow N_2 + N_2^+$ | Charge exchange |

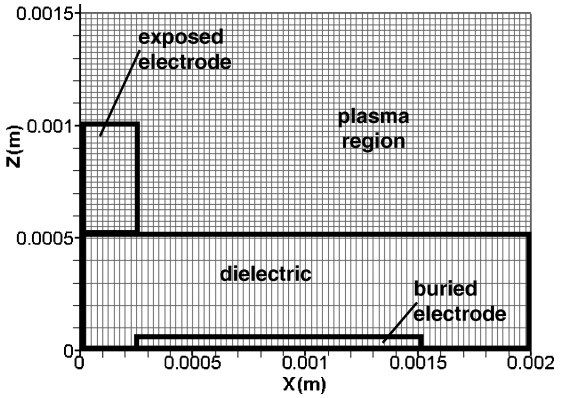


**Fig. 3 Computational geometry.**

The computational geometry is shown in Fig. 3. It consists of two electrodes separated by a dielectric. The upper electrode is 0.5 mm thick and protrudes only 0.25 mm into the computational domain. Initially a larger exposed electrode was utilized, but the plasma was found not to exist significantly beyond the right edge of the electrode. For this reason, the exposed electrode was shortened. The buried electrode is 1.25 mm long and is a boundary condition below the dielectric. The dielectric is 0.5 mm thick. The computational domain is 1.5 mm high $\times$ 2.0 mm long $\times$ 0.1 mm wide.

The grid is $165 \times 320$ cells. In the plasma region, the cells are $6.25 \times 10^{-6}$ m square (height and length) $\times$ 0.1 mm wide. Only every fourth cell in the plasma region is shown in the figure for clarity. The electrode and dielectric thicknesses are chosen to be representative of the experimental setups currently under investigation. The length of the buried electrode was shortened to decrease the computational work load. Longer electrodes can be used but were found unnecessary in the exploration of the discharge characteristics and force production mechanisms. The computational domain is one cell wide with reflective boundary conditions on either side. Therefore, although all particle motions and collisions are calculated in three dimensions, this is effectively only a two-dimensional simulation. The actual plasma is composed of numerous electron streamers, which are intrinsically three dimensional. Because the streamers move out from a wide electrode, however, the effect on the air is largely two dimensional, and the results of the computation should still be useful for understanding the force production mechanisms.

Particle boundary conditions were as follows: particles exiting the computational domain were deleted from the computation. Particles striking the exposed electrode would be neutralized and, therefore, were also deleted from the simulation. Particles striking the dielectric were held at the dielectric boundary, and their velocity was set to zero. In the actual plasma, an electron or an ion can bury itself into the dielectric as a result of the impact momentum. This can affect the speed at which the particles leave the dielectric when the electric field reverses because some energy has to be expended to extract them from the surface. It would also affect the timing of their departure because the electric field has to rise above some threshold for extraction. No attempt to model this has yet been made in the current simulation.

Electrical boundary conditions were as follows: The potential gradient was set to zero along the plasma boundaries. The potential was computed by solving the Poisson's equation throughout the domain, including the dielectric. The dielectric constant is currently

set to 1.0. The buried electrode was held at 0 V, whereas the exposed electrode was held at either 5000 or $-5000$ V. A time-varying potential was attempted, but because the electron avalanche takes only $10 \times 10^{-9}$ to $20 \times 10^{-9}$ s and the collision frequency with the neutrals forces a time step of about $1 \times 10^{-13}$ s, attempting to capture a single bias cycle is prohibitively expensive. Instead, the potential of the exposed electrode was set to $-5000$ V, and the discharge was computed until it extinguished. This was followed by setting the potential to 5000 V and, again, computing the discharge until it extinguishes. Therefore, the simulation utilizes a square wave input to the electrodes.

Different grid densities were tried for the simulation. The cell size in the plasma region was reduced from $2.5 \times 10^{-5}$ to $0.4 \times 10^{-5}$ m until the force began to converge. Further reductions were not made because of computational constraints.

The simulations were started by seeding the flow with a small number of electrons. Trials were conducted where the number of seed electrons was reduced until the discharge became independent of the size of the seed. This is a standard technique in this type of simulation.[14,15] The seed electrons are placed near the upper corner of the exposed electrode, where field effect electron emission is expected. The plasma discharge then evolves self-consistently as the electrons accelerate in the electric field and cause further ionization, dissociation, etc.

## III. Computational Results

Simulations were conducted of a two-dimensional slice of a dielectric barrier discharge at atmospheric pressure and density with a square wave input of amplitude 5000 V. The bias cycle frequency is not specified but is low enough to allow the discharge to extinguish before it reverses polarity. In the present simulation, this results in an effective frequency in the 1–10-MHz range.

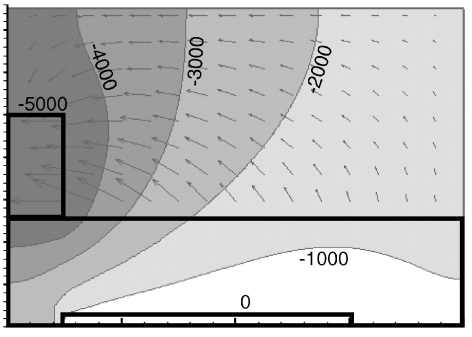


**Fig. 4 Electric potential (V) and electric field vectors at $t = 0.0$ s.**

The initial electric potential and electric field vectors are shown in Fig. 4. As expected, the potential contours are widely spaced away from the electrodes and show a large gradient where the electrodes are closest to each other. Generally, the electric field points from the buried electrode to the exposed electrode. The vector lengths are proportional to the electric field magnitude. The maximum field magnitude is about $7.3 \times 10^6$ V/m, and it occurs near the lower edge of the exposed electrode. At the right edge of the computational domain, the field strength is only about $1.0 \times 10^6$ V/m. The contours are continuous across the dielectric/vacuum interface because of the present choice of the dielectric constant.

### A. Initial Plasma Discharge: Forward Stroke

The charged particle density throughout the first 30 ns is shown in Fig. 5. The electrons accelerate along the electric field lines (tangent to the field vectors) and cause further ionizations as they stream toward the buried electrode. Note that the head of the avalanche is predominantly electrons, while the tail is predominantly ions. This occurs because of the high ambient neutral density. The ions, suffering numerous collisions with the neutrals, are halted from following the head of the streamer. The high-energy electrons continue forward, whereas the low-energy electrons remain with the ions. Such behavior has been observed before[19–22] and is typical of the Townsend phase of the streamer discharge. The energetic electrons stop their progress when they collide with the dielectric covering the buried electrode. In the figure this is indicated with the large negative charge density contours in the dielectric.

When a sufficient number of electrons strike the dielectric, the local vertical electric field is diminished. This results in subsequent electrons landing farther away from the exposed electrode (to the right in the figure). Continuing the simulation forward in time from this point does not produce significant further ionization, dissociation, or excitation because most of the electrons are now resting on the dielectric. These electrons, therefore, no longer accelerate, gain energy, or collide with neutrals. In the experiment, light emissions would cease after this time because the nitrogen metastable lifetime is on the order of tens of microseconds at these pressure and density.[23] Therefore, the glow can persist after the ions and electrons are recombined. The lack of further ionization is clearly shown in Fig. 6, which displays the total number of computational particles (ions and electrons) as a function of time. New ionization events cease after about 30 ns.

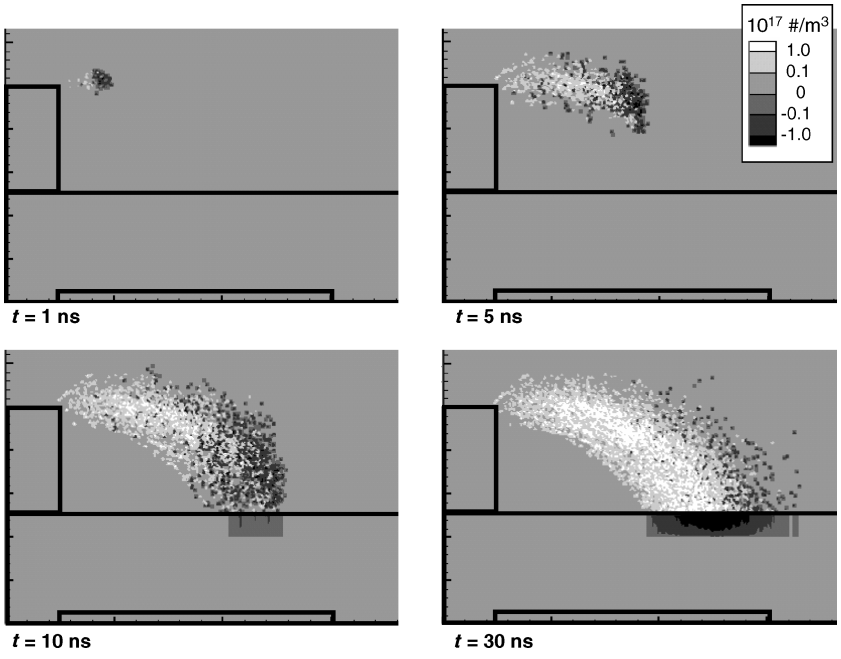


**Fig. 5 Charge density contours during forward stroke.**

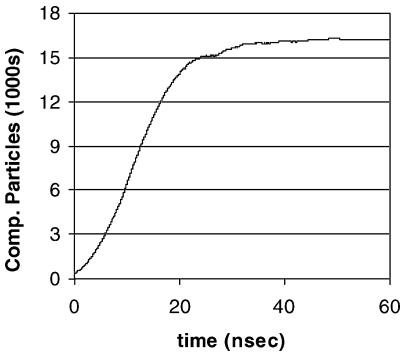


**Fig. 6 Computational particles during forward stroke. Ionization events stop after about 30 ns.**

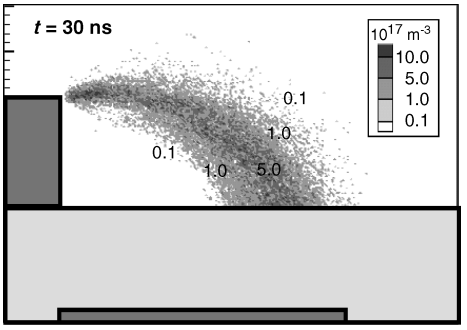


**Fig. 7 Dissociated nitrogen (N) density contours during forward stroke.**

In addition to ionization, the electrons accelerating in the electric field also produced dissociation and excitation of the molecular nitrogen. Figure 7 displays the atomic nitrogen density contours that result from dissociation collisions at time = 30 ns. The atomic-nitrogen contours follow the path of the discharge producing an area with a density of about $10^{17}$#/m$^3$. Also left in the wake of the discharge are large amounts of excited molecular nitrogen, shown in Fig. 8 for the same time in the discharge. The light emission from the plasma observed in the experiments is most closely associated with this species because it will release a photon when it deexcites.

### B. Reverse Plasma Discharge: Backstroke

At time = 60 ns the electrode bias was reversed, and computations were continued for another 60 ns. This gives an effective frequency of about $8 \times 10^6$ Hz. This is much larger than in the experiments, but it is still useful in shedding light on the nature of the plasma discharge. The important similarity maintained between the experiments and the computations is that for both the ionization events have effectively ceased before the field reverses.

As soon as the electric field is reversed, the electrons that have been resting up against the dielectric during the forward stroke start to accelerate back toward the exposed electrode and begin to again ionize, dissociate, and excite the molecular nitrogen. The charge density contours for the backstroke or second half of the bias cycle are shown in Fig. 9 for various points in time. The electrons leave the dielectric (the dark cloud in the figure) and begin moving toward the exposed electrode. The ions, because the exposed electrode is at 5000 V during the second half of the bias cycle, will now be pushed toward the dielectric. By $t = 65$ ns, some electrons have already hit the exposed electrode and left the plasma (because of neutralization). The ion density has risen from an average of $1 \times 10^{17}$ to $5 \times 10^{17}$ #/m$^3$. Five nanoseconds later (at $t = 70$ ns), the bulk of the electrons have reached the exposed electrode and the ion density contours peak at $1 \times 10^{18}$ #/m$^3$. At $t = 120$ ns the peak ion density is above $3 \times 10^{18}$ #/m$^3$. The time average ion density over the entire computational domain is $6 \times 10^{16}$ #/m$^3$ (as a result of large regions without any ions). During the forward stroke, however, the time average ion density is only $4 \times 10^{15}$ #/m$^3$. The results, therefore, show that the average ion density during the backstroke is at least

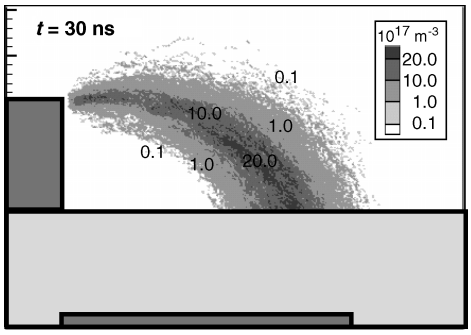


**Fig. 8 Excited nitrogen ($N_2^*$) density contours during forward stroke.**

10 times higher than the average ion density during the forward stroke. This is important because it is the ions that will be responsible for gaining momentum from the electric field force and imparting it to the ambient neutral flow.

Ionization in the forward stroke was largely over in the first 30 ns. In the backstroke, however, ionization had not halted after 60 ns ($t = 120$ ns). This is illustrated in Fig. 10, which shows the number of computational particles as a function of time. Throughout the entire half of the bias cycle, the amount of particles continued to grow, although the majority of the ionization occurs in the first 30 ns.

The extended period of ionization during the backstroke can be caused by a combination of factors. The plasma charge density during the backstroke is sufficiently large to change the global potential distribution and electric fields, shown in Fig. 11. The maximum electric field above the dielectric during the backstroke is about $5.5 \times 10^6$ V/m, whereas during the forward stroke the maximum electric field was $7.3 \times 10^6$ V/m. This could translate to smaller electron acceleration, which would take longer to reach energies capable of ionization. In addition, the backstroke is starting its avalanche with a vastly larger number of electrons. This alone will lead to a larger amount of ionization.

The difference in the length of the ionization periods between the forward and the backstrokes might suggest a way to make the method more efficient. If the backstroke leads to greater ion densities and longer periods of ionization, it might be advantageous to choose a bias cycle profile where the backstroke is longer than the forward stroke. For example, the time during which the potential of the exposed electrode is positive could be made longer than the time during which it is negative.

The density contours, at $t = 120$ ns, for dissociated (atomic) nitrogen and excited nitrogen are shown in Figs. 12 and 13, respectively. The atomic nitrogen (N) density levels have soared to above $1 \times 10^{19}$ #/m$^3$. This magnitude is a factor of 10 higher than the atomic-nitrogen magnitudes on the forward stroke of the discharge. The excited nitrogen levels are also a factor of 10 higher than the levels during the forward stroke. Comparing Figs. 8 and 13 reveals a curious behavior that has also been experimentally observed. The plasma glow is observed[6] farther from the exposed electrode on the backstroke than on the forward stroke. Simulations show the same behavior, when excited nitrogen is considered as the species responsible for emission. Figure 8 showed that the excited nitrogen reached the end of the buried electrode during the forward stroke. Figure 13 shows that, during the backstroke, the excited nitrogen reaches significantly beyond the end of the buried electrode. This behavior can be caused by several reasons: electrons landing beyond the end of the electrode might have been repelled and, therefore, decelerated by the electrons already on the dielectric. This would leave them with insufficient energy to cause further nitrogen excitation. Alternatively, electrons landing beyond the buried electrode might simply have been born and landed on the dielectric before having a sufficient time to gain energy and cause molecular excitation. In either case, when the electric field reverses during the backstroke, these electrons, which landed beyond the buried electrode, accelerate and gain sufficient energy to cause excitation and plasma light emission from a larger region.

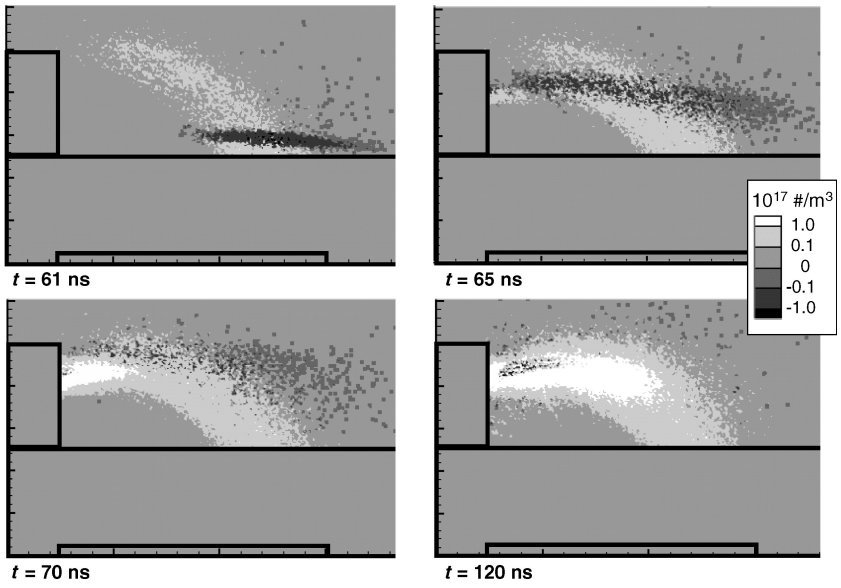


**Fig. 9 Charge density contours during backstroke.**

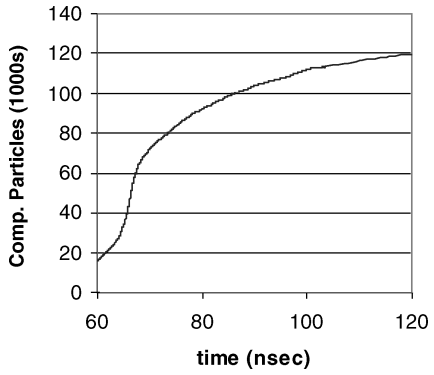


**Fig. 10 Computational particles during backstroke. Ionization events have not halted after 120 ns.**

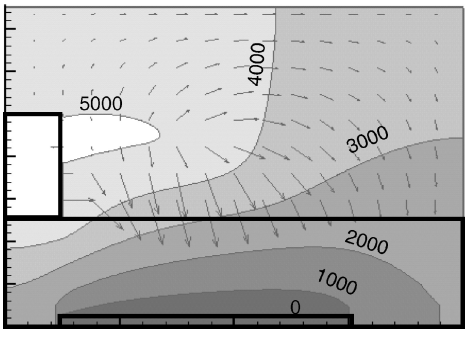


**Fig. 11 Electric potential (V) and electric field vectors at $t = 120.0$ s.**

### C. Force Production Mechanism

In the preceding sections, the charged particle densities and the plasma products were discussed. It was noted that the ion density was a factor of 10 higher during the backstroke than during the forward stroke. In this section, the significance of this asymmetry to the force production will be explored.

Figure 14 shows the vectors of force imparted by the ions to the neutrals at $t = 60$ ns. Note that, although the electron avalanche during the forward stroke is toward the buried electrode, the force imparted to the nitrogen is toward the exposed electrode. This occurs because the ions are forced toward the exposed electrode by the −5000-V bias and the resulting electric field. Averaging the force in the $x$ direction on the neutrals over the entire domain during the

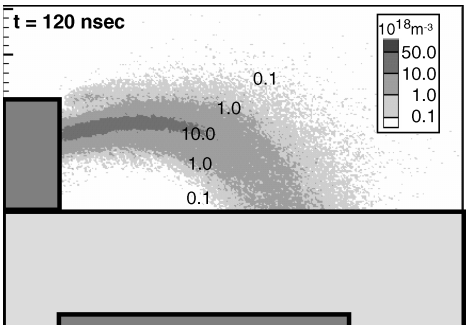


**Fig. 12 Dissociated nitrogen (N) density contours during backstroke.**

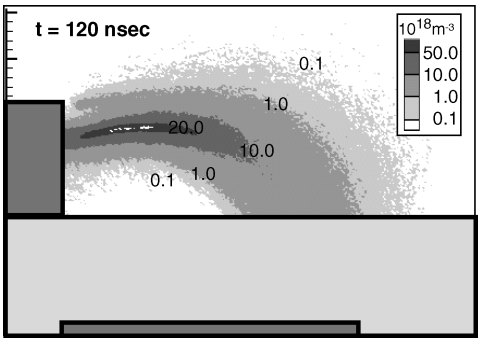


**Fig. 13 Excited nitrogen ($N_2^*$) density contours during backstroke.**

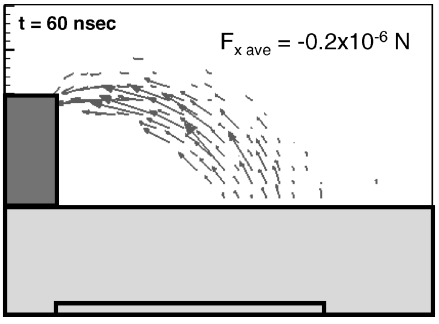


**Fig. 14 Vectors of momentum transfer to the neutrals at the end of the forward stroke.**

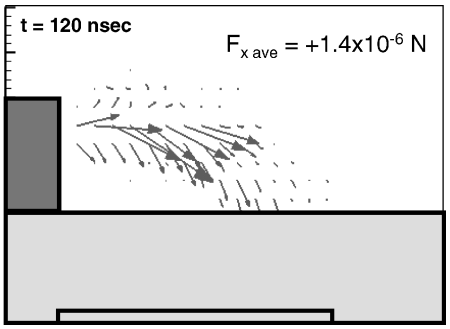


**Fig. 15 Vectors of momentum transfer to the neutrals at the end of the backstroke.**

forward stroke results in a net force of $-0.2 \times 10^{-6}$ N. This force is, as the vectors indicate, toward the exposed electrode.

Figure 15 shows the vectors of force imparted by the ions to the neutrals at $t = 120$ ns. During the backstroke, the electrons avalanche toward the exposed electrode, but the ions are pulled toward the buried electrode by the electric field. The net force on the neutrals, therefore, is directed toward the buried electrode. The average force in the $x$ direction over the domain and during the entire backstroke is $1.4 \times 10^{-6}$ N. This is seven times greater and in the opposite direction than during the forward stroke. The force is greater during the backstroke because of the disproportionately larger ion density.

Averaging the force over the entire electrode bias cycle (forward and backstrokes) gives a net force of $6.0 \times 10^{-7}$ N in the direction of the buried electrode. Therefore, the plasma actuator appears to produce a net force away from the exposed electrode and toward the buried electrode because of the larger production of ions during the second half of the bias cycle.

To make a sanity check, the force will be compared to a similar experiment. The current simulation results are generated with a power utilization of about 20 W. Reference 6 reports a force of 0.0013–0.0020 N for a plasma actuator operating at 20 W. The experimental actuator was 250 mm wide (dimension into the page on Fig. 3). Because the simulations represent a two-dimensional slice, which is only 0.1 mm wide, the total computational force for an actuator with a width equal to the experimental actuator would be 0.0015 N. Therefore, the computations appear to be in the correct neighborhood. This serves as a sanity check only because the simulations do not include the oxygen negative ion chemistry present in the air and the bias frequencies do not match. Nevertheless, this gives confidence to the results of the simulations.

These computations were carried out over a single electrode bias cycle only. However, because the plasma is extinguished at the end of each half of the bias cycle, the simulations should be representative of the physics occurring during all bias cycles. At the beginning of each cycle (during the forward stroke), the avalanche is begun with very few electrons present. The subsequent avalanche toward the buried electrode produces many electrons that halt their motion at the dielectric. The second half of the bias cycle (the backstroke) begins with all of the electrons produced during the forward cycle present. Therefore, the ionization will always be greater during the backstroke. At the end of the backstroke, almost all of the electrons enter the exposed electrode leaving the next bias cycle to begin, again, with relatively few electrons. The larger ion density during the backstroke will always produce a net force away from the exposed electrode and toward the buried electrode because that is the direction of the force on the ions. If both electrodes were covered with a dielectric, the forward and backavalanches would be symmetric and the net force should be zero. This, in fact, was tried in experiments carried out in Ref. 6. The authors report that, when both electrodes were covered by a dielectric, the force was not measurable. Smoke flow showed that some force, apparently smaller than the accuracy of the experimental apparatus, still forced the air in one direction. Therefore, some component of the force can still be caused by the electric field gradient or some, as of yet, unexplored mechanism.

## IV. Summary

Plasma actuators have demonstrated the ability to promote attachment of the flow around airfoils by providing momentum to the boundary layers. The method by which the momentum is imparted to the flow was the subject of the present study. A plasma actuator was simulated using PIC-DSMC methods at atmospheric pressure for a pure nitrogen flow. The electrodes were biased using a square-wave function with a frequency of 8 MHz. Both the electrons and ions were modeled as computational particles. The electric field was determined self-consistently during each time step. Collisions were resolved with the neutrals allowing for ionization, dissociation, and metastable excitation. The results show that the actuator works as a dielectric barrier discharge, in which the plasma is created through an electron avalanche. The ions gain momentum by accelerating in the electric field and, then, produce a force by transferring this momentum to the neutrals through collisions. Because the electric field reverses during the electrode bias cycle, the ions impart momentum in one direction during the first half of the cycle and in the opposite direction during the second half. The actuator produces a net force in one direction because the avalanche is not symmetric during both halves of the bias cycle. All of the electrons produced during the first half of the bias cycle are still on the surface of the dielectric at the beginning of the second half of the cycle. This results in ionization during the second half of the cycle that is more than 10 times greater than that produced during the first half. The electrons generated during the second half of the cycle are eventually lost to the exposed (conducting) electrode. Therefore, the next bias cycle has to begin the process from scratch (with almost no electrons). The result is that the ion density during the second half of the cycle is always greater than during the first half. The force is, consequently, greater for the second half of the cycle. In this manner, the plasma actuator produces a net force that should always be directed away from the exposed electrode.

## References

[1]Roth, J. R., Sherman, D. M., and Wilkinson, S. P., "Boundary Layer Flow Control with a One Atmosphere Uniform Glow Discharge Surface Plasma," AIAA Paper 98-0328, 1998.

[2]Hultgren, L. S., and Ashpis, D. E., "Demonstration of Separation Delay with Glow-Discharge Plasma Actuators," AIAA Paper 2003-1025, 2003.

[3]Huang, J., Corke, T. C., and Thomas, F. O., "Plasma Actuator for Separation Control of Low-Pressure Turbine Blades," *AIAA Journal*, Vol. 44, No. 1, 2006, pp. 51–57.

[4]Post, M., and Corke, T., "Separation Control on High Angle of Attack Airfoil Using Plasma Actuators," *AIAA Journal*, Vol. 42, No. 11, 2004, pp. 2177–2184.

[5]Enloe, C. L., McLaughlin, T. E., Van Dyken, R., Kachner, K. D., Jumper, E. J., Corke, T. C., Post, M., and Haddad, O., "Mechanisms and Responses of a Single Dielectric Barrier Plasma Actuator: Geometric Effects," *AIAA Journal*, Vol. 42, No. 3, 2004, pp. 595–604.

[6]Enloe, C. L., McLaughlin, T. E., Van Dyken, R., Kachner, K. D., Jumper, E. J., and Corke, T. C., "Mechanisms and Responses of a Single Dielectric Barrier Plasma Actuator: Plasma Morphology," *AIAA Journal*, Vol. 42, No. 3, 2004, pp. 589–594.

[7]Lieberman, M. A., and Lichtenberg, A. J., *Principles of Plasma Discharges and Materials Processing*, Wiley, New York, 1994, Chaps. 1 and 11.

[8]Sankaranarayanan, R., Pashaie, B., and Dhali, S. K., "Characteristics of a Barrier Discharge in Monatomic and Molecular Gases," *Applied Physics Letters,* Vol. 74, No. 21, 1999, pp. 3119–3121.

[9]Kang, W. S., Kim, Y., and Hong, S. H., "Spatio-Temporal Images of Single Streamer Propagation in Dielectric Barrier Discharge," *IEEE Transactions on Plasma Science,* Vol. 30, No. 1, 2002, pp. 166, 167.

[10]Liu, S., and Neiger, M., "Excitation of Dielectric Barrier Discharges by Unipolar Submicrosecond Square Pulses," *Journal of Physics D*, Vol. 34, 2001, pp. 1632–1638.

[11]Gibalov, V. I., and Pietsch, G. J., "The Development of Dielectric Barrier Discharges in Gas Gaps and on Surfaces," *Journal of Physics D*, Vol. 33, 2000, pp. 2618–2636.

[12]Birdsall, C. K., and Langdon, A. B., *Plasma Physics via Computer Simulation*, Adam Hilger, Bristol, England, U.K., 1991, Chap. 9.

[13]Kunhardt, E. E., and Tzeng, Y., "Role of Electron-Molecule Angular Scattering in Shaping the Electron-Velocity Distribution," *Physical Review A*, Vol. 34, No. 3, 1986, pp. 2158–2167.

[14]Kunhardt, E. E., and Tzeng, Y., "Development of an Electron Avalanche and Its Transition into Streamers," *Physical Review A*, Vol. 38, No. 3, 1988, pp. 1410–1421.

[15]Li, J., and Dhali, K., "Simulation of Microdischarges in a Dielectric–Barrier Discharge," *Journal of Applied Physics*, Vol. 82, No. 9, 1997, pp. 4205–4210.

[16]Font, G. I., and Boyd, I. D., "DSMC-PIC Simulation of a Helicon Etch Reactor and Comparison with Experiments," *Process Control, Diagnostics, and Modeling in Semiconductor Manufacturing*, edited by M. Meyyappan, D. J. Economou, and S. W. Butler, Electrochemical Society, Montreal, 1997, pp. 275–285.

[17]VanGilder, D. B., Font, G. I., and Boyd, I. D., "Hybrid Monte Carlo Particle-in-Cell Simulation of an Ion Thruster Plume," *Journal of Propulsion and Power*, Vol. 15, No. 4, 1999, pp. 530–538.

[18]Phelps, A. V., and Pichford, L. C., "Anisotropic Scattering of Electrons by $N_2$ and Its Effects on Electron Transport," JILA Information Center, Rept. 26, Univ. of Colorado, 1985; also *Physical Review A*, Vol. 31, 1985, pp. 2932–2949.

[19]Vitello, P. A., Penetrante, B. M., and Bardsley, J. N., "Simulation of Negative-Streamer Dynamics in Nitrogen," *Physical Review E*, Vol. 49, No. 6, 1994, pp. 5574–5598.

[20]Braun, D., Gibalov, V., and Pietsch, G., "Two-Dimensional Modeling of the Dielectric Barrier Discharge in Air," *Plasma Sources Science and Technology*, Vol. 1, 1992, pp. 166–174.

[21]Gibalov, V., and Pietsch, G., "The Development of Dielectric Barrier Discharges in Gas Gaps and on Surfaces," *Journal of Physics D,* Vol. 33, 2000, pp. 2618–2636.

[22]Massines, F., Rabedhi, A., Decomps, P., Ben Gadri, R., Segur, P., and Mayoux, C., "Experimental and Theoretical Study of a Glow Discharge at Atmospheric Pressure Controlled by Dielectric Barrier," *Journal of Applied Physics*, Vol. 83, No. 6, 1998, pp. 2950–2957.

[23]Ekey, R. C., and McCormack, E. F., "A Planar Jet Expansion Discharge Source of Molecular Afterglow Emission," *Chemical Physics Letters*, Vol. 381, No. 3, 2003, pp. 416–421.

M. Auweter-Kurtz
*Associate Editor*